SO264 SONNE-EMPEROR:
The Plio/Pleistocene to Holocene development of the pelagic North Pacific

D. Nürnberg[1], R. Tiedemann[2], L. Lembke-Jene[2], L. Jacobi[1], W.-S. Chao[2], Th. Frederichs[3]

[1]GEOMAR Hemholtz Centre for Ocean Research Kiel, Kiel, Germany
[2]Alfred-Wegener-Institut Hemholtz-Zentrum für Polar- und Meeresforschung, Bremerhaven, Germany
[3]Universität Bremen, Fachbereich Geowissenschaften, Bremen, Germany

As part of SO264 SONNE-EMPEROR, climate proxy time series were compiled from unique sediment cores from 2-2.5 km water depths along the **Emperor Seamount Chain** in the N-Pacific (~30˚N to ~50˚N. The proxy time series reflect temporal and spatial changes in the pelagic subtropical and subarctic N-Pacific gyres over the last ~3.5 million years.

We achieved a dynamic and three-dimensional understanding of the long-term, natural development of climate states, their coupling to regional and supra-regional climate changes, and the associated complex atmospheric-oceanic circulation patterns and interactions in the N-Pacific. As these time series are largely unaffected by near-land processes, they will be more reliable for the assessment of ocean-climate models.

N-Pacific affected by W-Pacific Warmpool

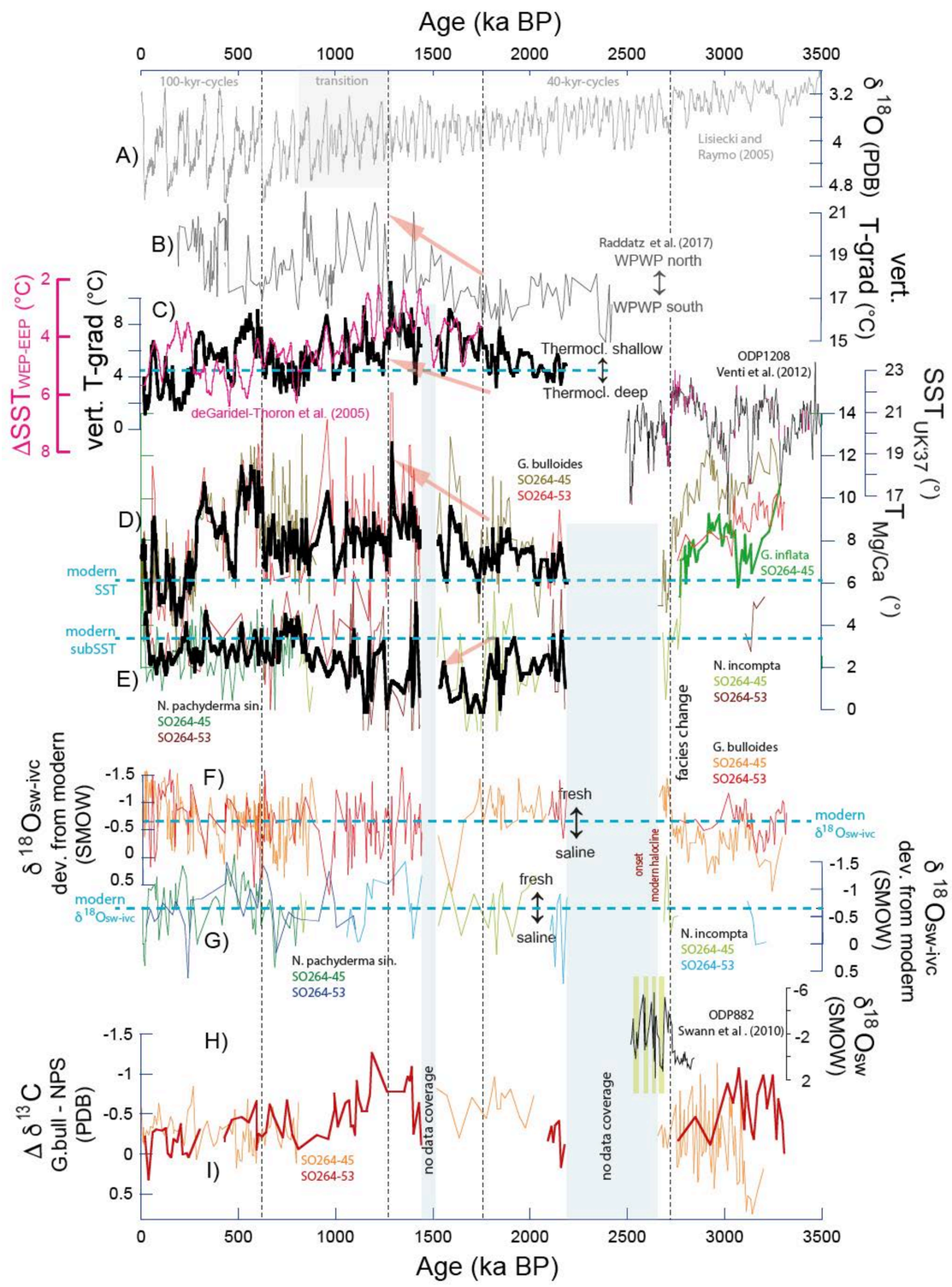

Combined proxy records of cores SO264-45 and -53 of the last ~3.4 Ma compared to reference data sets. A) LR04 $\delta^{18}O$ climate record (Lisiecki & Raymo, 2005); B) Vertical temperature gradient in the W-Pacific Warm Pool (WPWP; Raddatz et al., 2017) with gradual northward shift of the WPWP from ~1.7-1.35 Ma BP (red arrow). C) Vertical temperature gradient (ΔT) at the Emperor Seamounts (~47˚N) with thermocline shoaling from ~1.7-1.3 Ma BP (red arrow). Blue dashed line = present-day SST-subSST gradient. The ΔT record largely corresponds to changes in the W-E-directed SST gradient (ΔSST, pink; de Garidel-Thoron et al., 2005) in the equatorial Pacific. D) Surface temperatures (SST from $Mg/Ca_{G.bulloides}$; brown: core -45; red: core -53) with $SST_{Mg/Ca}$ mean (black) compared to the ODP Site 1208 $SST_{UK'37}$ record (Venti et al., 2012). E) Subsurface temperatures (subSST from $Mg/Ca_{N.pachyderma}$ and $Mg/Ca_{N.incompta}$, green: core -45; black: core -53) with $subSST_{Mg/Ca}$ mean (black). Red arrows mark significant trends in $SST_{Mg/Ca}$ and $subSST_{Mg/Ca}$. Blue dashed lines = present-day SST and subSST. F) Surface $\delta^{18}O_{sw\text{-}ivc}$ data series (ice volume-corrected seawater $\delta^{18}O$ values; $\delta^{18}O_{sw\text{-}ivc}$; from Mg/Ca and $\delta^{18}O$ of *G. bulloides*; orange: core -45; red: core -53) as approximation of salinity. Negative $\delta^{18}O_{sw\text{-}ivc}$ values indicate lower salinities. G) Subsurface $\delta^{18}O_{sw\text{-}ivc}$ data series (from Mg/Ca and $\delta^{18}O$ of *N. pachyderma* sin. and *N. incompta*; green: core -45; blue: core -53). The $\delta^{18}O_{sw\text{-}ivc}$ data series in F) and G) are shown as deviations from the current surface and subsurface $\delta^{18}O_{sw\text{-}ivc}$ values (blue dashed lines; $\delta^{18}O_{sw}$ measured on SO264 water samples; Prof. Dr M. Kienast, Halifax, Canada; unpublished). H) $\delta^{18}O_{sw}$ reconstruction of ODP Site 882 based on siliceous diatoms (Swann et al., 2010). I) $\delta^{13}C$ gradient between *G. bulloides* and *N. pachyderma* sin. or *N. incompta* (orange = SO264-45; red = SO264-53).

El Niño-like conditions

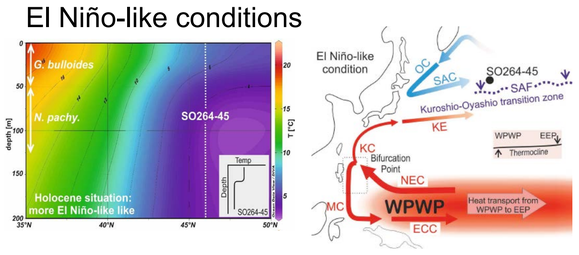

La Niña-like conditions

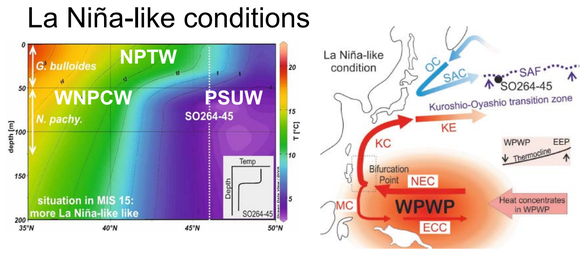

Subtropical: North Pacific Tropical Water (NPTW); Western North Pacific Central Water (WNPCW)
Subarctic: Pacific Subarctic Upper Water PSUW

Outcome

~3.3–2.73 Ma. Northward expanded North Pacific Tropical Water (NPTW) in line with displacement of subtropical and subpolar gyres.

at ~2.73 Ma. Cooling due to southward retreat of subtropical watermasses (NPTW) and strong influence of subpolar water masses (PSUW). Increasing seasonality?

~2.1-1.7 Ma. Seasurface warming accompanied by subsurface cooling during times of stable and deep halocline.

~1.7-1.3 Ma. Shallow thermocline due to (seasonal?) northward expansion of a shallow tongue of subtropical above subarctic watermasses. Increased heat transport via intensified Kuroshio Current likely caused by changes in SST gradient between WPWP and eq. E-Pacific.

~1.3- <0.7 Ma. Glacial/interglacial migrations of Kuroshio-Oyashio extension zone. Thermocline deepening synchronised with northward expansion of WPWP and increasing meridional SST gradients between WPWP and eq. E-Pacific.

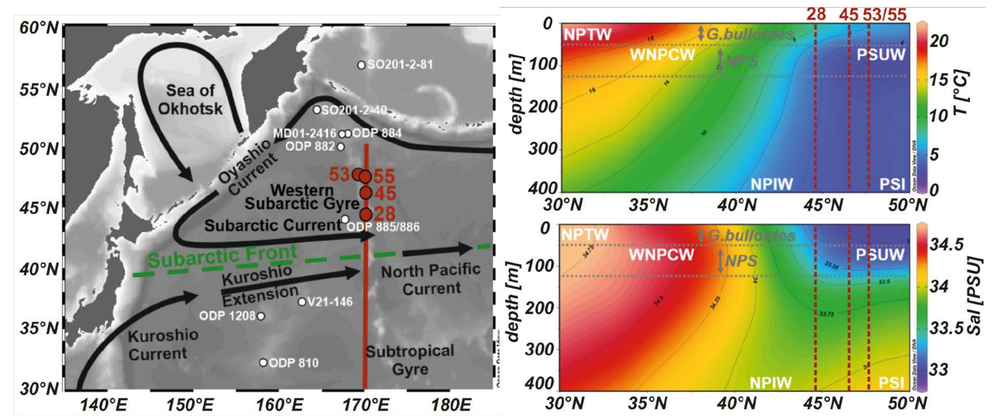

Approach: Age models of sediment cores SO264-28, -45, -53 and -55 are based on litho-, benthic oxygen isotope-, magneto-, bio- and tephro-stratigraphic approaches. The cores have very low sedimentation rates and date back to ~3.5 million years. The presence of hiata in an area with high relief energy and erosive bottom currents afford consideration.

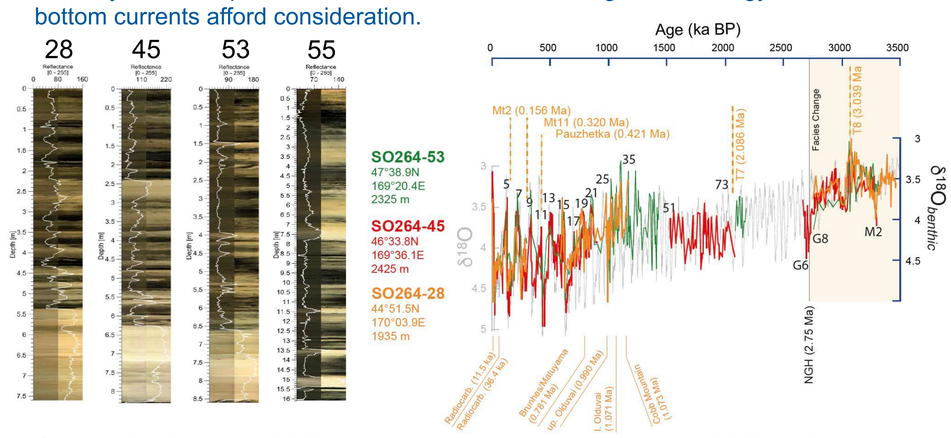

Approach: Surface (SST) and **sub**surface temperature (subSST) and salinity ($\delta^{18}O_{seawater}$) reconstructions over the last ~3.5 Ma, derived from Mg/Ca and stable oxygen isotopes ($\delta^{18}O$) of planktic foraminifers.

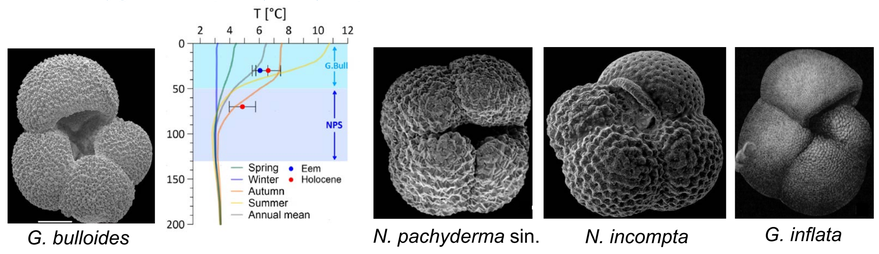

G. bulloides | *N. pachyderma* sin. | *N. incompta* | *G. inflata*

Approach: Marine productivity and eolian (dust) transport were reconstructed from sedimentary Ca/Ti, Ba/Ti (XRF-scanner), and XRF-Fe-data. Ice-rafted debris (IRD) is defined as lithogenic sediment components >400 µm.

Marine productivity and dust flux

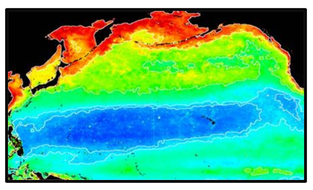

Chlorophyll a concentration (oceantracks.org)

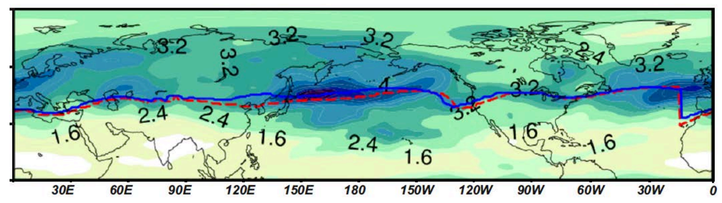

Distribution of summer "transient eddy kinetic energy" (m^2/s^2), showing the axis of the Westwind Drift at 200 hPa (red stippled line; Xu et al., 2020)

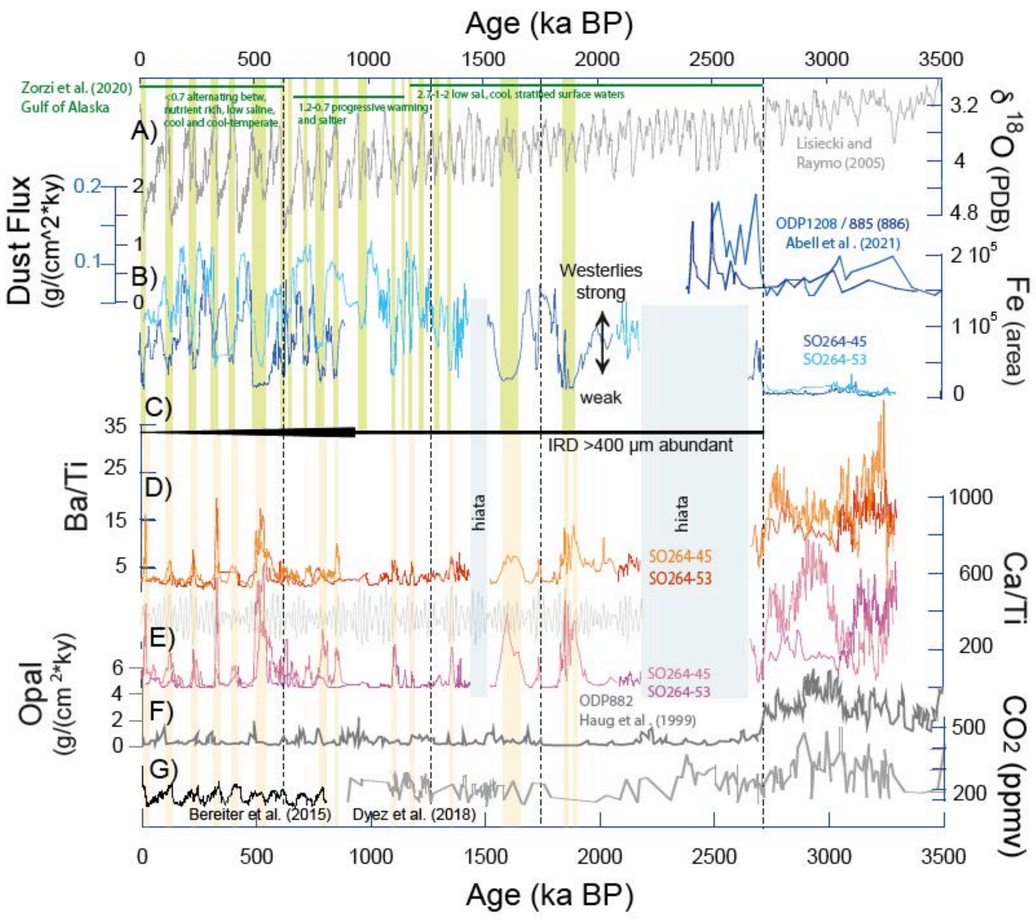

Combined proxy records of cores SO264-45 and -55 of the last ~3.4 Ma compared to reference data sets. A) LR04 $\delta^{18}O$ climate record (Lisiecki & Raymo, 2005); B) Fe (light blue = core -53; dark blue = core -45) shows the variability of the aeolian dust input and thus changes in the westerly wind drift (cf. Lamy et al., 2004). Phases of low Fe input, predominantly during warm periods, are highlighted in green. In comparison, the dust inputs at ODP Sites 1208 and 885/886 (Abell et al., 2021; cf. Fig. III-1) are shown; C) Ice-rafted debris (IRD; defined as >400 µm, non-basaltic, partly rounded, lithogenic sediment components). D) Ba/Ti (red = core -53; orange = core -45) and E) Ca/Ti (violet = core -53; dark red = core -45) reflect changes in marine productivity (cf. Nürnberg & Tiedemann, 2004; Riethdorf et al., 2013a). Phases of increased productivity (shaded orange) appear predominantly during deglaciations and early interglacials. Summer insolation at ~47˚N (~380-480 W/m^2) lies between the element records (grey; Paillard et al., 1996). F) Biogenic silica accumulation rates (Haug et al., 1999; ODP Site 882). G) Atmospheric CO_2 (Bereiter et al., 2015; Dyez et al., 2018). Green notes from Zorzi et al. (in press) regarding ODP Site 887 (Gulf of Alaska).

Outcome

Continuous ice-transport since 2.73 Ma

Low productivity after 2.73 Ma due to strong halocline, high nutrient utilization

High productivity **during deglaciations, early interglacials** -> fueling from below?

High Fe-flux due to strong westerlies **during cool periods**, lagging productivity